The transition redshift as a probe of reionization

Angus Beane,[1][*] Adam Lidz,[2] Kana Moriwaki,[3] and others

[1]*Center for Astrophysics | Harvard & Smithsonian, 60 Garden Street, Cambridge, MA 02138, USA*
[2]*Department of Physics & Astronomy, University of Pennsylvania, 209 South 33rd Street, Philadelphia, PA 19104, USA*
[3]*Department of Physics, The University of Tokyo, 7-3-1 Hongo, Bunkyo, Tokyo 113-0033, Japan*

ABSTRACT

The early stages of the Epoch of Reionization (EoR), probed by the 21 cm line, are sensitive to the detailed formation of the first galaxies. An important transition occurs on large scales at $z \sim 10$, when the 21 cm field transitions from being positively correlated with the density field to being negatively correlated. The redshift at which this transition occurs (the "transition redshift") is in principle measurable if the 21 cm field can be cross-correlated with a tracer of the density field (such as galaxies or a line intensity map) at that high redshift. Since the transition redshift is derived from a cross-correlation, it is in principle sensitive to the structure of both the 21 cm field and the tracer used to measure it. However, by considering a fixed model for the EoR and varying the parameters of a simple model for a Hα intensity map cross-correlation, we show that the transition redshift is in fact very insensitive to the structure of the density tracer. A simple analytic argument motivates this result. We show that prospects for measuring the transition redshift are feasible in the near-term with a combination of LOFAR and JWST. Being derived from a cross-correlation, the transition redshift is less impacted by foreground contamination currently inhibiting 21 cm auto-spectrum measurements. Therefore, the transition redshift is an interesting probe of the early stages of the EoR, and its detectability and interpretability deserve further study.

Key words: cosmology: theory – dark ages, reionization, first stars – large-scale structure of Universe

1 INTRODUCTION

The redshifted 21 cm line contains a great deal of information about the structure and evolution of the Epoch of Reionization (EoR). Once measured at $z \sim 6$–12, it should reveal the nature of the formation of the first stars, galaxies, and black holes, as well as the large-scale structure of the Universe at high redshift (Loeb & Furlanetto 2013). While instruments have reached the sensitivity necessary to detect the signal during the EoR, issues of foreground contamination and instrumental artifacts have so far prevented the success of such efforts. Only upper limits have been placed on the amplitude of the 21 cm fluctuations (e.g. Paciga et al. 2013; Dillon et al. 2014; Beardsley et al. 2016; Patil et al. 2017).

Because of the great difficulties confronting 21 cm auto-spectrum measurements, the prospect of measuring 21 cm in cross-correlation with another tracer of large-scale structure, such as galaxies. The galaxy field will only correlate with the cosmological 21 cm signal, and the foregrounds will not contribute to the mean signal (though they will make the measurement noisy, and so some foreground subtraction is still necessary).

The 21 cm-galaxy cross-correlation was first explored by Wyithe & Loeb (2007) in the context of using Lyα-emitters to distin-

guish between "inside-out" and "outside-in" reionization scenarios. However, this technique is limited to the late stages of reionization since Lyα-emitters are obscured by neutral hydrogen even slightly earlier into the EoR (e.g. Kashikawa et al. 2006). Furlanetto & Lidz (2007) expanded upon this by considering a general galaxy survey. It was later shown that the scale at which the cross-correlation goes from negative to zero (the "turnover scale") provides a tracer of the bubble size. However, the precise turnover scale also depends on the properties of the selected galaxy sample, with turnover happening on larger scales if only more massive galaxies can be detected (Lidz et al. 2009). A number of authors have studied this cross-correlation in the context of detectability of the anti-correlation on large scales (Wiersma et al. 2013; Vrbanec et al. 2016; Hutter et al. 2017), and its dependence on the details of the EoR (Park et al. 2014).

In addition to the cross-correlation between 21 cm and galaxies, the cross-correlation between 21 cm and intensity maps has been investigated in an analogous fashion. Line intensity mapping experiments aim to measure the large-scale structure of emission in a certain line, and is easier to perform over a large area at high redshift than a galaxy survey. Current targets include [C II], CO, Lyα, and Hα (for a recent review, see Kovetz et al. 2017). Another intriguing possible line is [O III] 88 μm (e.g. Moriwaki et al. 2018), in which a lensed $z = 9.1$ galaxy has recently shown to be exceptionally bright (Hashimoto et al. 2018).

[*] E-mail: angus.beane@cfa.harvard.edu

This cross-correlation was first studied with the CO rotational lines (Lidz et al. 2011), and then the [C II] (Gong et al. 2012) and Lyα lines (Silva et al. 2013). The possibility of using the cross-bispectrum the 21 cm and [C II] fields has been explored (Beane & Lidz 2018), along with combining the three cross-spectra with a 21 cm, [C II], and [O III] overlap (Beane et al. 2019). While in this work we will only consider the cross-correlation between 21 cm and galaxies, all of what we consider is applicable to the transition redshift as computed by cross-correlating 21 cm with any of these emission lines.

In the case of either galaxies or emission lines, it is expected that the two are positively correlated at the very beginning of the EoR (though the emission lines may be very weak due to the lack of significant metal enhancement). This is because the densest regions host the most mass and therefore 21 cm emission and galaxy populations. However, the densest regions will also ionize first **cite something**, and after some time 21 cm and galaxies will become negatively correlated. We refer to the redshift at which this transition occurs at a fixed k as the "transition redshift" $z_\star(k)$, assuming that only one such zero exists. In other words, the cross-correlation at k vanishes at $z = z_\star(k)$.

In this work we investigate to what extent the transition redshift is dependent upon the galaxy sample used to define it. We assume a galaxy catalog selected using an [O III] emitter survey. In particular, we are interested in how $z_\star$ changes as we vary the parameters of the [O III] luminosity-mass relation for a fixed halo catalog.

2   METHODS

2.1   The transition redshift

The transition redshift $z_\star(k)$ is defined by a field x which traces the density field on large scales and the condition that

$$P_{21,x}(k, z_\star(k)) \equiv 0. \tag{1}$$

If more than one such $z_\star$ exists, then we choose the lowest one where $P_{21,x}$ last transitioned from positive to negative.

2.2   21cmFAST

We generate realizations of the 21 cm field for our different EoR models using the publicly available code 21cmFAST v1.3[1]. Spin temperature fluctuations are computed and the excursion set approach is used to identify the ionized regions (Mesinger et al. 2011). Rather than using the mean collapsed fraction, we use the halo field to compute the ionization and 21 cm fields, since we are interested in the evolution at early redshifts where the Poisson statistics of the halo field can be important.

The parameters used in our 21cmFAST runs are as folows. The minimum halo mass contributing to the ionizing budget is $10^8 \, \mathrm{M_\odot}$. The H II efficiency factor (ζ) is set to 10. The maximum smoothing scale for the ionization field R_{max} (loosely referred to as the "mean-free path") is set to $30 \, \mathrm{Mpc}$, though this quantity has almost no effect on the early stage of the EoR. We set the fraction of baryons converted to stars ($f_\star$) to be 0.1. We ignore redshift-space distortions for convenience. All other parameters are set to their default values, except for the heating parameter discussed in the next paragraph. The

---

[1] https://github.com/andreimesinger/21cmFAST,   commit: 42e7566

exact parameter files are given in the github repository associated with this work (see the Supplementary Material).

Our three different models for the EoR differ in the efficiency of their heating, controlled by the number of X-ray photons per solar mass in galaxies (ζ_X). Our fiducial model (fid) is the default value $\zeta_X = 2 \times 10^{56}$, while our "hot" and "cold" models (hot and cold) set $\zeta_X = 10^{57}$ and 5×10^{55}, respectively. The average δT_b signal is shown in **some figure**, which shows **something**. Note that none of these models account for the recent claimed detection by the EDGES group of an extremely deep absorption trough at $z \sim 17$ (Bowman et al. 2018). If confirmed, though, that detection would indicate an extremely low gas temperature at $z \sim 17$, which would favor larger amplitudes of the spin temperature fluctuations at $z \sim 10$, unless heating were extremely efficient after $z \sim 17$. **don't know how I feel about the last sentence**

We generate the halo field using the included halo finder in 21cmFAST. This halo finder is a remnant of an earlier version of the code (Mesinger & Furlanetto 2007) and is typically unused in standard configurations. It is based upon the "peak-patch" algorithm for halo finding introduced by Bond & Myers (1996).

2.3   Intensity mapping

In order to model the relation between luminosity (L) and halo mass, we follow Beane et al. (2019). Specifically, we assume that the mean luminosity of a halo of mass M is,

$$\langle L \rangle(M) = L_0 \left[\frac{M}{M_0} \right]^\alpha, \tag{2}$$

where L_0/M_0^α is set to match the total average intensity of the line at that redshift and α is the power-law index. We then draw the luminosity of each halo from a lognormal distribution of mean $\langle L \rangle(M)$ and scatter σ. Once the average intensity is fixed (which we assume so), this is a two-parameter model (α and σ) of the luminosity-mass relation. In practice, the average intensity of the field only enters in the detectability calculation, so we instead work in the convenient units where $L_0 = 1$ and $M_0 = 10^{10} \, \mathrm{M_\odot}$.

We assign a luminosity to each halo according to this prescription. An important consideration is that we have not specified which line we are working with. In detail, the relationship between a halo and it's luminosity is a complicated function of the state of the interstellar medium of the hosted galaxy, which can depend upon a number of both deterministic and stochastic quantities. Our model crudely attempts to account for this by including some random scatter, but will ultimately be a rough description of reality.

Some words justifying why our simple model will extend to more complicated luminosity-halo relations.

3   RESULTS

3.1   The transition redshift

3.2   The halo field

If we switch to LIM I think this section should be scrapped, except showing ztran vs k but using LIM and density instead of halos

We first investigate the dependence of the transition redshift as defined by the halo field. Fig. 2 shows the transition redshift defined by the 21 cm – density cross-power spectrum (see Eq. 1) as a function of k. The three models considered in this work are shown in orange, gray, and teal (hot, fid, and cold, respectively).
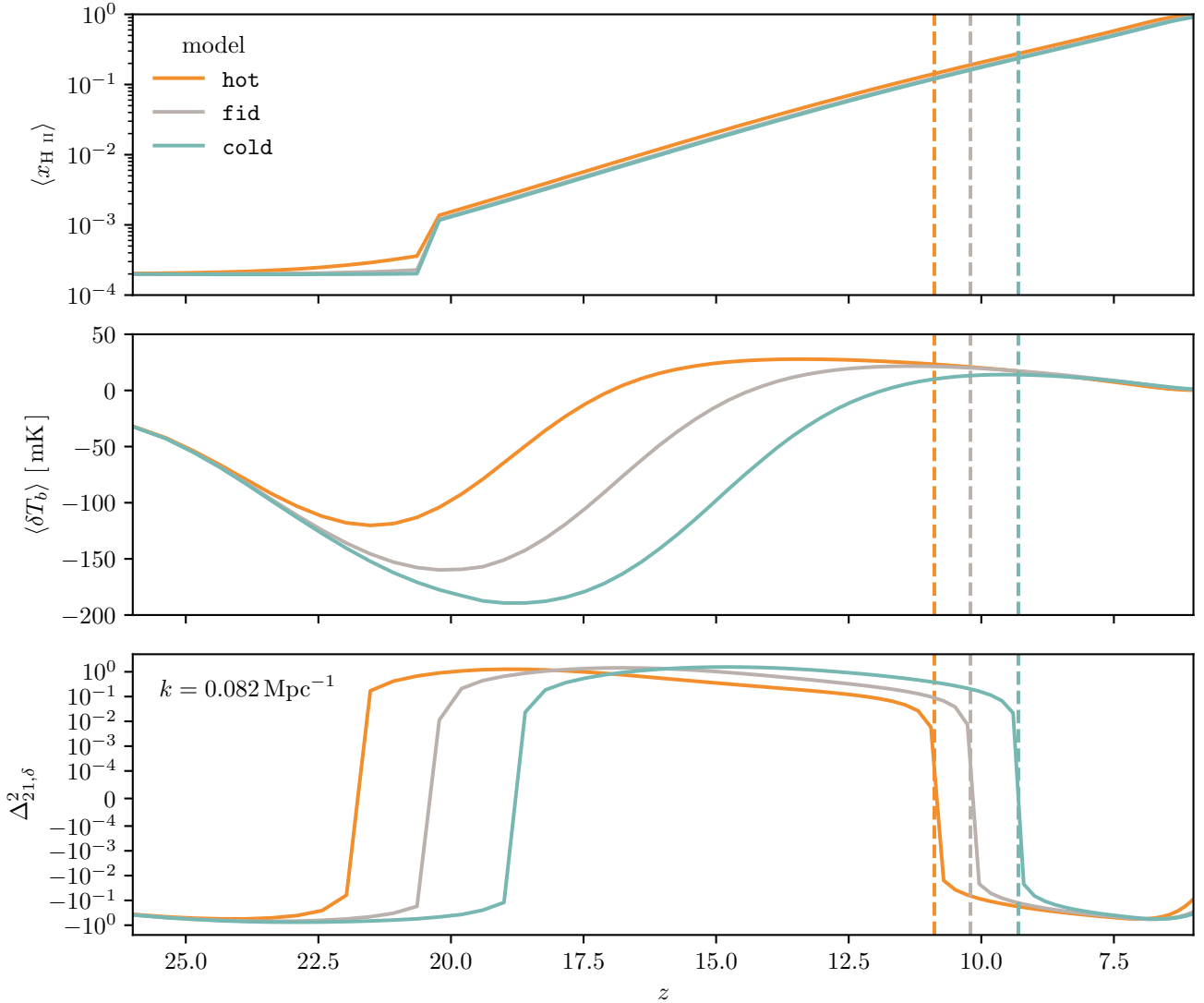
Figure 1. A summary of the ionization and heating history of our three EoR models: `hot`, `fid`, and `cold`. *Upper*: the ionization history of each model, showing that reionization begins ($\langle x_{\mathrm{H\,II}} \rangle \sim 0.01$) at $z \sim 16$ and ends at $z \sim 6$ in each model. In detail the ionization histories are slightly different, but not drastically. *Lower*: the heating history of each model, showing the strong differences in the monopole signal. The transition redshift $z_\star$ (defined where $P_{21,\delta}(z_\star) = 0$) for each model is shown as a vertically dashed line. We see that models in which heating is more efficient have an earlier $z_\star$.

Fig. 2 shows that $z_\star$ is only weakly a function of k.

3.3 Line-intensity mapping

We now turn to understanding how $z_\star$ depends on the parameters of our generic line-intensity mapping field: the slope (α) and lognormal scatter (σ). See § 2.3 for more details of the construction of the field.

In Fig. 4 we plot $z_\star$ as a function of each of these parameters – α and σ. We see that $z_\star$ is remarkably insensitive to the value of either of these parameters, with some small deviation as a function of α. The `hot`, `fid`, and `cold` models only vary by a total of 1.2%, 0.56%, 0.52% with respect to α, and 0.070%, 0.10%, and 0.11% with respect to σ, respectively.

4 DETECTABILITY

Up to this point, we have not been specific about which galactic emission line one might consider using to measure $z_\star$ – in fact, our entire formalism could be executed using a galaxy survey, if one with sufficient redshift accuracy and depth could be executed. While it will not be possible for a traditional galaxy survey to extend to $z \sim 10$ in the near future, it may be possible to execute a survey of line-emitting galaxies, e.g., with [O III]-emitters (Moriwaki et al. 2018, 2019).

In this work we will consider the prospect of performing intensity mapping measurements of the Hα line using the proposed, space-based Cosmic Dawn Intensity Mapper (CDIM) (Cooray et al. 2019). CDIM is an infrared telescope with an 83 cm dish capable of measuring $R = 300$ spectra from wavelengths 0.75 μm to 7.5 μm. Therefore, CDIM will be able to measure the H-α line (656 nm)
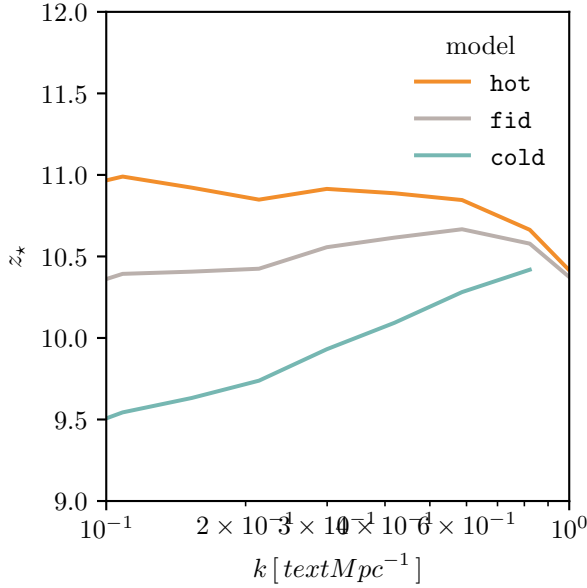
Figure 2. The transition redshift ($z_\star$) as defined by cross-correlating with the density field (solid lines) and all resolved halos (dashed lines, $M \gtrsim 5 \times 10^9\,\mathrm{M_\odot}$), for our three different EoR models (`hot`, `fid`, and `cold`). We see that $z_\star$ is only a mild function of k for the three models, with slightly stronger dependence as the heating of the model decreases. The most dependence comes in the `cold` model, where $z_\star$ changes by $\sim 7\,\%$ from $k = 0.1$ to $0.6\,h\,\mathrm{Mpc}^{-1}$. **Some words for why cold and fid cut off at some k**

Figure 3. The transition redshift ($z_\star$) as defined by cross-correlating with the halo field for our three different EoR models (`hot`, `fid`, and `cold`) as a function of the cut-off mass. The cross-correlation is only made between the 21 cm field and all halos with masses $M > M_{\rm cut}$. One can see that for the `fid` and `cold` models, $z_\star$ is only mildly a function of $M_{\rm cut}$ below a certain cut-off mass ($\sim 10^{10.5}\,\mathrm{M_\odot}$ in both models). In other words, as long as a galaxy survey is deep enough so as to resolve a sufficient number of galaxies, the $z_\star$ is not dependent on the depth of the survey. The `hot` model shows more dependence, but this may be due to sampling noise due to the smaller number of such halos at the higher $z_\star$ typical for the `hot` model.

from $z = 0.14$ to 10.4 and the H-β line ($486\,\mathrm{nm}$) from $z = 0.54$ to 14.4, so long as there is a detectable signal. CDIM will execute a wide, medium, and deep survey of 311, 31.1, and $15.6\,\mathrm{deg}^2$, respectively. However, only the medium survey's field will overlap with 21 cm experiments (HERA and a deep field from SKA1-LOW). Therefore we will only consider the medium survey.

We choose to study the H-α and H-β lines since the uncertainty regarding their total intensity at $z \sim 10$ should be less uncertain than for lines that require metal enrichment such as [C II], [O III], or [N II], since the total metal enrichment of the universe is quickly declining at these high z

We assume a linear relationship between H-α luminosity and star formation rate (Kennicutt 1998):

$$
\begin{aligned}
L_{\mathrm{H}\alpha} &= 3.29 \times 10^7 \left(\frac{\mathrm{SFR}}{1\,\mathrm{M_\odot\,yr^{-1}}} \right) L_\odot \\
&\equiv L_{0,\mathrm{H}\alpha} \left(\frac{\mathrm{SFR}}{1\,\mathrm{M_\odot\,yr^{-1}}} \right)
\end{aligned}
\tag{3}
$$

This relation is based on a Salpeter IMF and is calibrated towards local galaxies. As discussed in Katz et al. (2019), the reality of $z \sim 10$ galaxies may be slightly different – the IMF may be more top heavy, and the metal-poor nature of a typical star will naturally produce more ionizing photons. However, the escape of ionizing photons may be more efficient at higher redshift, and the conventional relation assumes no escape. Katz et al. (2019) provide a slightly shallower fitting form for the $L_{\mathrm{H}\alpha} - \mathrm{SFR}$ relation based upon their simulations, but we choose to use the conventional relation here.

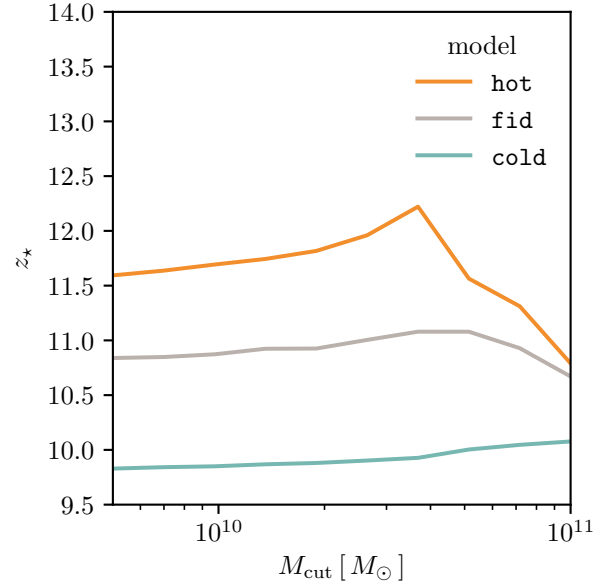We use a fitting formula for the SFRd calibrated upon galaxies

from $z = 0$ to 8 (Madau & Dickinson 2014)

$$
\psi(z) = 0.015 \frac{(1 + z)^{2.7}}{1 + [(1 + z)/2.9]^{5.6}}\,\mathrm{M_\odot yr^{-1} Mpc^{-3}}.
\tag{4}
$$

The comoving emissitivity of the Hα line can then be readily computed as,

$$
\epsilon_{\mathrm{H}\alpha}(z) = L_{0,\mathrm{H}\alpha}\psi(z).
\tag{5}
$$

The average specific intensity can be computed from the comoving emissitivity as (Lidz et al. 2011; Pullen et al. 2013),

$$
\langle I_{\mathrm{H}\alpha}\rangle(z) = \frac{\epsilon_{\mathrm{H}\alpha}(z)}{4\pi\nu_{\mathrm{rest,H}\alpha}} \frac{c}{H(z)}
\tag{6}
$$

The variance per mode of the cross-spectrum between the 21 cm field and a line i is given by (e.g. Furlanetto & Lidz 2007)

$$
\mathrm{Var}[P_{21,i}] = P_{21,i}^2 + P_{21,\mathrm{tot}}P_{i,\mathrm{tot}},
\tag{7}
$$

where $P_{21,\mathrm{tot}} = P_{21,21} + N_{21}$, where N_{21} is the total noise contribution. $P_{i,\mathrm{tot}}$ is defined similarly.

In detail the surface brightness sensitivity will have a frequency-dependent structure, but for $z \sim 9$ to 10, it is reasonable to assume a conservative, constant value of $\sigma_{\mathrm{H}\alpha} \sim 4 \times 10^4\,\mathrm{Jy/sr}$ for the medium survey. To convert the surface brightness sensitivity to a power spectrum noise, we simply write,

$$
N_{\mathrm{H}\alpha} = \sigma_{\mathrm{H}\alpha}^2 V_{\mathrm{voxel}},
\tag{8}
$$

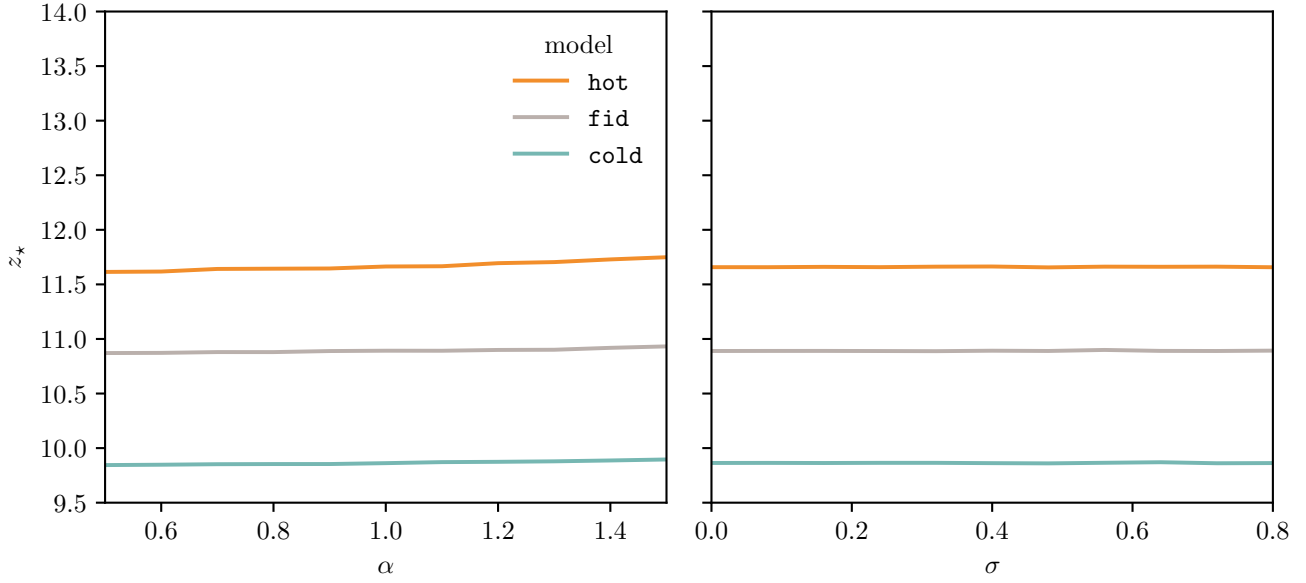where V_{voxel} is the comoving volume of one voxel. To compute this

Figure 4. The transition redshift ($z_\star$) defined by cross-correlating with a generic two-parameter intensity mapping field. The parameter α sets the slope of the luminosity-mass relation and the parameter σ sets the lognormal scatter in this relation (see § 2.3). The hot, fid, and cold models only vary by a total of 1.2%, 0.56%, 0.52% with respect to α, and 0.070%, 0.10%, and 0.11% with respect to σ, respectively. Clearly $z_\star$ varies only with the structure of the 21 cm field, and is thus an excellent probe of reionization.

we use the fact that CDIM will have $1''$ pixels and a resolution of $R = 300$.

For N_{21}, we assume that $N_{21} = P_{21,21}(k = 0.1\,\mathrm{Mpc}^{-1})$, a reasonable approximation given that HERA-350 will image some large scale modes (DeBoer et al. 2017), as discussed previously (Beane & Lidz 2018).

The number of modes is given by,

$$N_m = \frac{4\pi k^2 \delta k}{V_{\mathrm{fund}}},\tag{9}$$

where δk is the width of the k-bin and V_{fund} is the volume of a fundamental mode. We assume a square survey area, and so this is given by,

$$V_{\mathrm{fund}} = \frac{(2\pi)^3}{L_\perp^2 L_\parallel},\tag{10}$$

where $L_\perp$ is the and $L_\parallel$ is the comoving length of the redshift extent of the bin. The optimal redshift binning is not entirely clear, since the observational target is not the power spectrum. We assume a redshift bin of $\Delta z = 0.03$, which is smaller than the expected error we compute on $z_\star$, and so is not an unreasonable choice. We assume a k-bin of fairly large width, from $k = 0.1$ to $0.4\,\mathrm{Mpc}^{-1}$.

By expanding $P_{21,\mathrm{H}\alpha}$ as a linear function about $z_\star$, we can estimate the error on $z_\star$ by

$$\mathrm{Var}[z_\star] = \left(\left.\frac{\partial P_{21,\mathrm{H}\alpha}}{\partial z}\right|_{z_\star}\right)^{-2} \mathrm{Var}[P_{21,\mathrm{H}\alpha}],\tag{11}$$

where $\partial P_{21,\mathrm{H}\alpha}/\partial z$ is computed numerically.

5 CONCLUSIONS

The conclusions.

REFERENCES

Beane A., Lidz A., 2018, ApJ, 867, 26
Beane A., Villaescusa-Navarro F., Lidz A., 2019, ApJ, 874, 133
Beardsley A. P., et al., 2016, ApJ, 833, 102
Bond J. R., Myers S. T., 1996, ApJS, 103, 1
Bowman J. D., Rogers A. E. E., Monsalve R. A., Mozdzen T. J., Mahesh N., 2018, Nature, 555, 67
Cooray A., et al., 2019, arXiv e-prints, p. arXiv:1903.03144
DeBoer D. R., et al., 2017, PASP, 129, 045001
Dillon J. S., et al., 2014, Phys. Rev. D, 89, 023002
Furlanetto S. R., Lidz A., 2007, ApJ, 660, 1030
Gong Y., Cooray A., Silva M., Santos M. G., Bock J., Bradford C. M., Zemcov M., 2012, ApJ, 745, 49
Hashimoto T., et al., 2018, Nature, 557, 392
Hutter A., Dayal P., Müller V., Trott C. M., 2017, ApJ, 836, 176
Kashikawa N., et al., 2006, ApJ, 648, 7
Katz H., et al., 2019, MNRAS, 487, 5902
Kennicutt Robert C. J., 1998, ARA&A, 36, 189
Kovetz E. D., et al., 2017, arXiv e-prints, p. arXiv:1709.09066
Lidz A., Zahn O., Furlanetto S. R., McQuinn M., Hernquist L., Zaldarriaga M., 2009, ApJ, 690, 252
Lidz A., Furlanetto S. R., Oh S. P., Aguirre J., Chang T.-C., Doré O., Pritchard J. R., 2011, ApJ, 741, 70
Loeb A., Furlanetto S. R., 2013, The First Galaxies in the Universe
Madau P., Dickinson M., 2014, ARA&A, 52, 415
Mesinger A., Furlanetto S., 2007, ApJ, 669, 663
Mesinger A., Furlanetto S., Cen R., 2011, MNRAS, 411, 955
Moriwaki K., et al., 2018, MNRAS, 481, L84
Moriwaki K., Yoshida N., Eide M. B., Ciardi B., 2019, arXiv e-prints, p. arXiv:1906.10863

Paciga G., et al., 2013, MNRAS, 433, 639
Park J., Kim H.-S., Wyithe J. S. B., Lacey C. G., 2014, MNRAS, 438, 2474
Patil A. H., et al., 2017, ApJ, 838, 65
Pullen A. R., Chang T.-C., Doré O., Lidz A., 2013, ApJ, 768, 15
Silva M. B., Santos M. G., Gong Y., Cooray A., Bock J., 2013, ApJ, 763, 132
Vrbanec D., et al., 2016, MNRAS, 457, 666
Wiersma R. P. C., et al., 2013, MNRAS, 432, 2615
Wyithe J. S. B., Loeb A., 2007, MNRAS, 375, 1034

APPENDIX A: SOME EXTRA MATERIAL

The appendix.

This paper has been typeset from a TEX/LATEX file prepared by the author.